CORA Cork Open Research Archive
Cartlann Taighde Oscailte Chorcaí

Title	Microscopic processes in global relativistic jets containing helical magnetic fields: dependence on jet radius
Authors	Nishikawa, Ken-Ichi;Mizuno, Yosuke;Gómez, Jose L.;Duțan, Ioana;Meli, Athina;White, Charley;Niemiec, Jacek;Kobzar, Oleh;Pohl, Martin;Pe'er, Asaf;Frederiksen, Jacob Trier;Nordlund, Åke;Sol, Helene;Hardee, Philip E.;Hartmann, Dieter H.
Publication date	2017
Original Citation	Nishikawa, K.-I., Mizuno, Y., Gómez, J., Duțan, I., Meli, A., White, C., Niemiec, J., Kobzar, O., Pohl, M., Pe'er, A., Frederiksen, J., Nordlund, Å., Sol, H., Hardee, P. and Hartmann, D. (2017) 'Microscopic processes in global relativistic jets containing helical magnetic fields: dependence on jet radius', Galaxies, 5(4), 58 (7pp). doi: 10.3390/galaxies5040058
Type of publication	Article (peer-reviewed)
Link to publisher's version	http://www.mdpi.com/2075-4434/5/4/58 - 10.3390/galaxies5040058
Rights	© 2018, the Authors. Licensee MDPI, Basel, Switzerland. This article is an open access article distributed under the terms and conditions of the Creative Commons Attribution (CC BY) license (http://creativecommons.org/licenses/by/4.0/). - http://creativecommons.org/licenses/by/4.0/
Download date	2024-03-29 07:42:46
Item downloaded from	https://hdl.handle.net/10468/6345

UCC
University College Cork, Ireland
Coláiste na hOllscoile Corcaigh

galaxies

MDPI

Article

Microscopic Processes in Global Relativistic Jets Containing Helical Magnetic Fields: Dependence on Jet Radius

Ken-Ichi Nishikawa [1,*], Yosuke Mizuno [2], Jose L. Gómez [3], Ioana Duţan [4], Athina Meli [5,6], Charley White [1,7,†], Jacek Niemiec [8], Oleh Kobzar [8], Martin Pohl [9,10], Asaf Pe'er [11], Jacob Trier Frederiksen [12], Åke Nordlund [13], Helene Sol [14], Philip E. Hardee [15] and Dieter H. Hartmann [16]

1 Department of Physics, University of Alabama in Huntsville, ZP12, Huntsville, AL 35899, USA; cmw0037@uah.edu
2 Institute for Theoretical Physics, Goethe University, D-60438 Frankfurt am Main, Germany; mizuno@th.physik.uni-frankfurt.de
3 Instituto de Astrofísica de Andalucía, CSIC, Apartado 3004, 18080 Granada, Spain; jlgomez@iaa.csic.es
4 Institute of Space Science, Atomistilor 409, RO-077125 Bucharest-Magurele, Romania; ioana.dutan@gmail.com
5 Department of Physics and Astronomy, University of Gent, Proeftuinstraat 86, B-9000 Gent, Belgium; ameli@ulg.ac.be
6 Department of Physics and Astronomy, University of Liege, Place du 20-Août, 7, 4000 Liège, Belgium
7 Department of Physics, Florida State University, 600 W, College Avenue Tallahassee, FL 32306, USA
8 Institute of Nuclear Physics PAN, ul. Radzikowskiego 152, 31-342 Kraków, Poland; Jacek.Niemiec@ifj.edu.pl (J.N.); oleh.kobzar@ifj.edu.pl (O.K.)
9 Institut fur Physik und Astronomie, Universität Potsdam, 14476 Potsdam-Golm, Germany; pohlmadq@gmail.com
10 DESY, Platanenallee 6, 15738 Zeuthen, Germany
11 Physics Department, University College Cork, T12 YN60 Cork, Ireland; a.peer@ucc.ie
12 Innofactor Denmark A/S, Telia Parken, Øster Allé 48, 2100 København Ø, Denmark; jacob.trier@innofactor.com
13 Niels Bohr Institute, University of Copenhagen, Blegdamsvej 17, DK-2100 København, Denmark; aake@nbi.dk
14 LUTH, Observatore de Paris-Meudon, 5 place Jules Jansen, CEDEX 92195 Meudon, France; helene.sol@obspm.fr
15 Department of Physics and Astronomy, The University of Alabama, Tuscaloosa, AL 35487, USA; pehardee@gmail.com
16 Department of Physics and Astronomy, Clemson University, Clemson, SC 29634, USA; hdieter@g.clemson.edu
* Correspondence: ken-ichi.nishikawa@nasa.gov; Tel.: +1-256-824-2593
† Affiliation 7 is the current address.

Academic Editor: Emilio Elizalde
Received: 23 August 2017; Accepted: 22 September 2017; Published: 26 September 2017

Abstract: In this study, we investigate the interaction of jets with their environment at a microscopic level, which is a key open question in the study of relativistic jets. Using small simulation systems during past research, we initially studied the evolution of both electron–proton and electron–positron relativistic jets containing helical magnetic fields, by focusing on their interactions with an ambient plasma. Here, using larger jet radii, we have performed simulations of global jets containing helical magnetic fields in order to examine how helical magnetic fields affect kinetic instabilities, such as the Weibel instability, the kinetic Kelvin–Helmholtz instability (kKHI) and the mushroom instability (MI). We found that the evolution of global jets strongly depends on the size of the jet radius. For example, phase bunching of jet electrons, in particular in the electron–proton jet, is mixed with a larger jet radius as a result of the more complicated structures of magnetic fields with excited kinetic instabilities.

In our simulation, these kinetic instabilities led to new types of instabilities in global jets. In the electron–proton jet simulation, a modified recollimation occurred, and jet electrons were strongly perturbed. In the electron–positron jet simulation, mixed kinetic instabilities occurred early, followed by a turbulence-like structure. Simulations using much larger (and longer) systems are required in order to further thoroughly investigate the evolution of global jets containing helical magnetic fields.

Keywords: relativistic jets; particle-in-cell simulations; global jets; helical magnetic fields; kinetic instabilities; kink-like instability; recollimation shocks; polarized radiation

1. Introduction

Relativistic jets are collimated plasma outflows associated with active galactic nuclei (AGN), gamma-ray bursts (GRBs), stellar-mass black holes, and pulsars (e.g., [1]). Among these astrophysical systems, blazars and GRB jets produce the most luminous phenomena in the universe (e.g., [2]). Despite extensive observational and theoretical investigations, including simulation studies, our understanding of their formation, interaction and evolution in ambient plasma, and consequently their observable properties, such as time-dependent flux and polarity (e.g., [3]), remains rather limited.

Astrophysical jets are ubiquitous in the universe and involve many essential/basic plasma phenomena, such as interaction with the interstellar medium, the generation of magnetic fields, turbulence, reconnection, and particle acceleration. Many of the processes that determine the behavior of large-scale relativistic jets are very complex, involving plasma physics and often coupling global, large-scale dynamics to microscopic processes that occur on short spatial and temporal scales associated with plasma kinetic effects. We carried out kinetic plasma simulations using our relativistic particle-in-cell (RPIC) code with the intent to advance our knowledge of global relativistic jets with helical magnetic fields and associated phenomena, such as particle acceleration, kinetic reconnection, and turbulence, which cannot be investigated with fluid models (i.e., relativistic magnetohydrodynamic (RMHD) simulations).

Recently, we performed global jet simulations involving the injection of a cylindrical non-magnetized jet into an ambient plasma in order to investigate shock (Weibel instability), and velocity shear instabilities (kKHI and mushroom instability (MI)) simultaneously [4]. In this paper, we describe the preliminary results of this study of global relativistic jets containing helical magnetic fields.

2. Simulation Setup

Jets powered by black holes, which are then injected into the ambient interstellar medium, contain magnetic fields that are thought to be helically twisted (e.g., [1]). On the basis of this understanding, we performed global simulations of jets containing helical magnetic fields injected into an ambient medium (e.g., [5,6]). The key issue we investigated was how the helical magnetic fields affect the growth of the kKHI, the MI, and the Weibel instability. RMHD simulations demonstrated that jets containing helical magnetic fields develop a kink instability (e.g., [7–9]). Because our RPIC simulations were large enough to include a kink instability, we found a kink-like instability in our electron–proton jet case.

2.1. Helical Magnetic Field Structure

In our simulations [5], cylindrical jets were injected with a helical magnetic field, implemented similarly to the RMHD simulations performed by Mizuno et al. [10]. Our simulations used Cartesian coordinates. Because the pitch profile parameter $\alpha = 1$, which gives constant magnetic pitch and

magnetic helicity, Equations (9)–(11) from [10] are reduced to Equation (1), and the magnetic field takes the following form:

$$B_x = \frac{B_0}{[1+(r/a)^2]}, \quad B_\phi = \frac{(r/a)B_0}{[1+(r/a)^2]} \tag{1}$$

The toroidal magnetic field is created by a current $+J_x(y,z)$ in the positive x-direction, so that it is defined in Cartesian coordinates by

$$B_y(y,z) = \frac{((z-z_{\rm jc})/a)B_0}{[1+(r/a)^2]}, \quad B_z(y,z) = -\frac{((y-y_{\rm jc})/a)B_0}{[1+(r/a)^2]}. \tag{2}$$

Here a is the characteristic length-scale of the helical magnetic field, $(y_{\rm jc},\, z_{\rm jc})$ is the center of the jet, and $r = \sqrt{(y-y_{\rm jc})^2+(z-z_{\rm jc})^2}$. The chosen helicity is defined through Equation (2), which has a left-handed polarity with positive B_0. At the jet orifice, we implemented the helical magnetic field without the motional electric fields. This corresponded to a toroidal magnetic field generated self-consistently by jet particles moving along the $+x$-direction.

2.2. Magnetic Fields in Helically Magnetized RPIC Jets with Larger Jet Radius

As an initial step, we examined how the helical magnetic field modifies the jet evolution using a small system before performing larger-scale simulations. A schematic of the simulation injection setup is given in our previous work [5]. In these small-system simulations, we utilized a numerical grid with $(L_x, L_y, L_z) = (645\Delta, 131\Delta, 131\Delta)$ (L: simulation system length; simulation cell size: $\Delta = 1$) and periodic boundary conditions in transverse directions with a jet radius $r_{\rm jt} = 20\Delta$. The jet and ambient (electron) plasma density measured in the simulation frame were $n_{\rm jt} = 8$ and $n_{\rm am} = 12$, respectively. This set of densities of jet and ambient plasmas was used in our previous simulations [4–6].

In the simulations, the electron skin depth was $\lambda_{\rm s} = c/\omega_{\rm pe} = 10.0\Delta$, where c is the speed of light, $\omega_{\rm pe} = (e^2 n_{\rm am}/\epsilon_0 m_{\rm e})^{1/2}$ is the electron plasma frequency, and the electron Debye length for the ambient electrons was $\lambda_{\rm D} = 0.5\Delta$. The jet-electron thermal velocity was $v_{\rm jt,th,e} = 0.014c$ in the jet reference frame. The electron thermal velocity in the ambient plasma was $v_{\rm am,th,e} = 0.03c$, and the ion thermal velocities were smaller by $(m_{\rm i}/m_{\rm e})^{1/2}$. The simulations were performed using an electron–positron ($e^{\pm}$) plasma or an electron–proton (e^-–p^+ with $m_{\rm p}/m_{\rm e} = 1836$) plasma for the jet Lorentz factor of 15 and with the ambient plasma at rest ($v_{\rm am} = 0$).

In the simulations, we used the initial magnetic field amplitude parameter $B_0 = 0.1c$ ($c = 1$), the magnetization parameter defined as the ratio between the electromagnetic field (EMF) energy flux to the plasma matter energy flux $\sigma = B^2/n_{\rm e}m_{\rm e}\gamma_{\rm jet}c^2 = 2.8\times10^{-3}$, and the characteristic magnetic radius of $a = 0.25\times r_{\rm jt}$. The helical field structure inside the jet was defined by Equations (1) and (2). For the external magnetic fields, we used a damping function $\exp[-(r-r_{\rm jt})^2/b]$ $(r \geq r_{\rm jt})$ that multiplies Equations (1) and (2) with the tapering parameter $b = 200$. The final profiles of the helical magnetic field components were similar to those of the case in which the jet radius was $r_{\rm jt} = 20\Delta$; the only difference was that $a = 0.25\times r_{\rm jt}$.

In this report, we maintain all the simulation parameters as described above, except the jet radius and simulation size (adjusted on the basis of the jet radius). We performed simulations with larger jet radii of $r_{\rm jt} = 40\Delta$, 80Δ, and 120Δ. In these small-system simulations, we utilized a numerical grid with $(L_x, L_y, L_z) = (645\Delta, 257\Delta, 257\Delta)$, $(645\Delta, 509\Delta, 509\Delta)$, $(645\Delta, 761\Delta, 761\Delta)$ (simulation cell size: $\Delta = 1$). The cylindrical jet with jet radii of $r_{\rm jt} = 40\Delta$, 80Δ, 120Δ was injected in the middle of the y–z plane ($(y_{\rm jc}, z_{\rm jc}) = (129\Delta, 129\Delta)$, $(252\Delta, 252\Delta)$, $(381\Delta, 381\Delta)$, respectively) at $x = 100\Delta$. The largest jet radius ($r_{\rm jt} = 120\Delta$) was larger than that in [4] ($r_{\rm jt} = 100\Delta$), but the simulation length was much shorter ($_x = 2005\Delta$).

Figure 1 shows the y-component of the magnetic field (B_y) in the jet radius with $r_{\rm jet} = 20\Delta$ and 80Δ. The initial helical magnetic field (left-handed; clockwise viewed from the jet front) was enhanced and disrupted as a result of the instabilities for both cases.

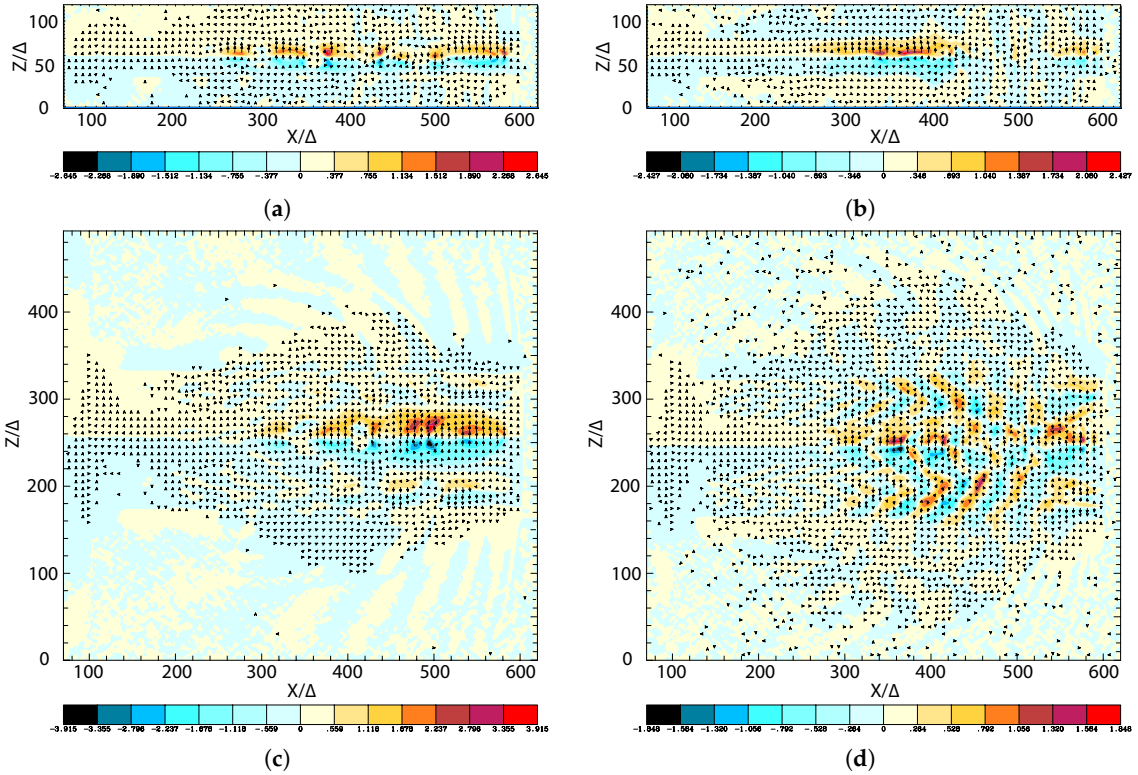


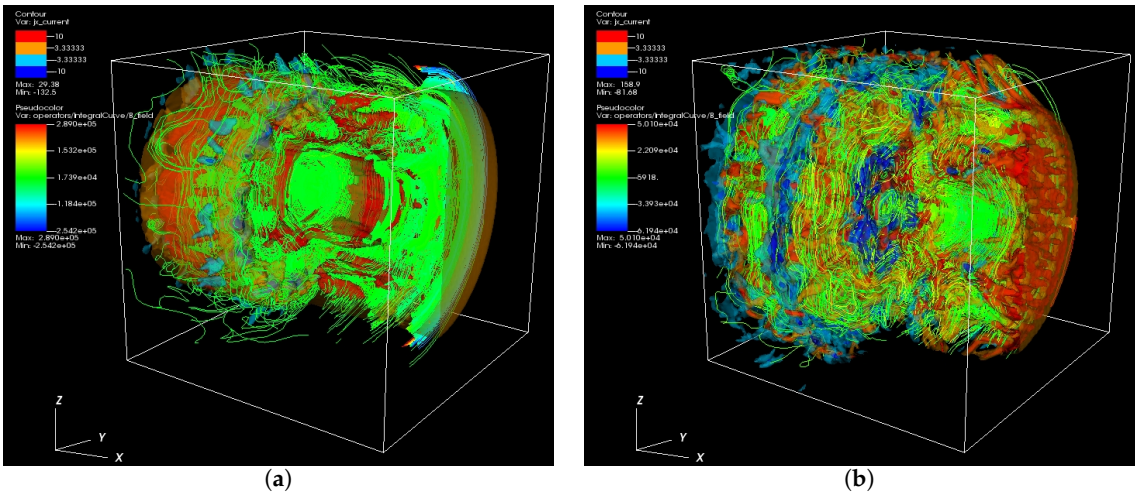
Figure 1. Isocontour plots of the azimuthal component of magnetic field B_y intensity at the center of the jets for e^-–p^+ (**a**,**c**) and $e^\pm$ (**b**,**d**) jets, with $r_{\rm jet} = 20\Delta$ (**a**,**b**) and $r_{\rm jet} = 80\Delta$ (**c**,**d**) at time $t = 500\omega_{\rm pe}^{-1}$. The disruption of helical magnetic fields was caused by instabilities and/or reconnection. The max/min numbers of panels are (**a**) ± 2.645, (**b**) ± 2.427, (**c**) ± 3.915, and (**d**) ± 1.848.

Even for shorter simulation systems, the growing instabilities were affected by the helical magnetic fields. These complicated patterns of $B_{\rm y}$ are generated by currents created by instabilities in jets. A larger jet radius provokes the growth of more modes of instabilities within jets, which make the jet structures more complicated. The simple recollimation shock generated in the small jet radius is shown in Figure 1a,b [5]. We need to perform longer simulations in order to investigate the full development of instabilities for jets with helical magnetic fields.

In order to investigate 3D structures of the averaged jet electron current ($J_{\rm x}$), we plotted it in the 3D ($420 \leq x/\Delta \leq 620$, $152 \leq y, z/\Delta \leq 352$) region of the jet front.

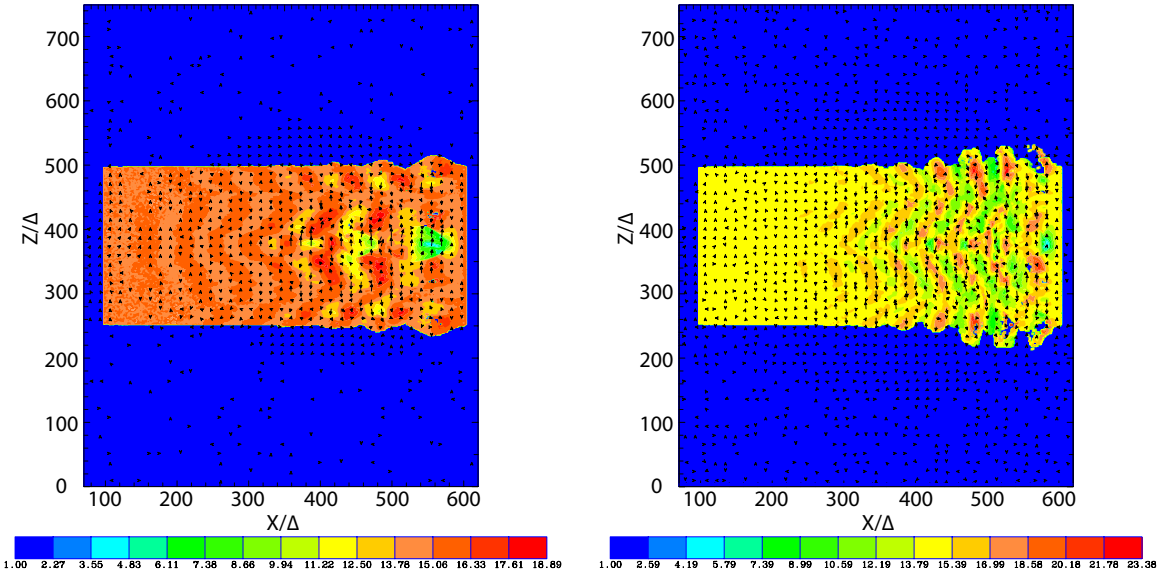
Figure 2 shows the current ($J_{\rm x}$) of jet electrons for e^-–p^+ (a) and $e^\pm$ (b) jets. The cross-sections at $x/\Delta = 520$, $y/\Delta = 252$ and the surfaces of jets show complicated patterns, which are generated by instabilities with the magnetic field lines.

In order to determine the particle acceleration, we calculated the Lorentz factor of jet electrons in the cases with $r_{\rm jet} = 120\Delta$, as shown in Figure 3. These patterns of the Lorentz factor coincided with the changing directions of local magnetic fields that were generated by instabilities. The directions of the magnetic fields are indicated by the arrows (black spots), which can be seen with magnification. The directions of the magnetic fields were determined by the generated instabilities. The structures at the edge of the jets were generated by the kKHI. The plots of the x-component of the current J_x in the y–z plane show the MI in the circular edge of the jets, as shown in Figure S1.



(**a**) (**b**)

Figure 2. Panels show 3D iso-surface plots of the current (J_x) of jet electrons for e^-–p^+ (**a**) and $e^\pm$ (**b**) jets with $r_{\rm jet} = 80\Delta$ at time $t = 500\omega_{\rm pe}^{-1}$. The lines show the magnetic field stream lines in the quadrant of the front part of the jets. Color scales for the contour (upper left) for (**a**,**b**) are red: 10; orange: 3.33; right blue: −3.33; blue: −10. The color scales of streaming lines are (**a**) (2.89, 1.53, 0.174, −1.2, −2.54) $\times 10^5$, and (**b**) (5.01, 2.21, −0.592, −3.39, −6.19) $\times 10^4$.



(**a**) (**b**)

Figure 3. Panels (**a**,**b**) show 2D plot of the Lorentz factor of jet electrons for e^-–p^+ (**a**) and $e^\pm$ (**b**) jets with $r_{\rm jet} = 120\Delta$ at time $t = 500\omega_{\rm pe}^{-1}$. The arrows (black spots) show the magnetic fields in the x–z plane.

In order to investigate 3D structures of the averaged jet-electron Lorentz factor, we plotted its iso-surface ($320 \leq x/\Delta \leq 620$, $381 \leq y, z/\Delta \leq 531$) of a quadrant of the jet front in 3D.

Figure 4 shows the Lorentz factor of jet electrons for e^-–p^+ (a) and $e^\pm$ (b) jets. The cross-sections and surfaces of the jets show complicated patterns that were generated by instabilities with the magnetic field lines.

In both cases with the jet radii larger than $r_{\rm jet} = 80\Delta$, the kKHI and MI were generated at the jet surfaces, and inside the jets, the Weibel instability was generated with kink-like instability, in particular in the electron–proton jet. We aim to investigate this further using different parameters, including a, which determines the structure of helical magnetic fields in Equations (1) and (2).

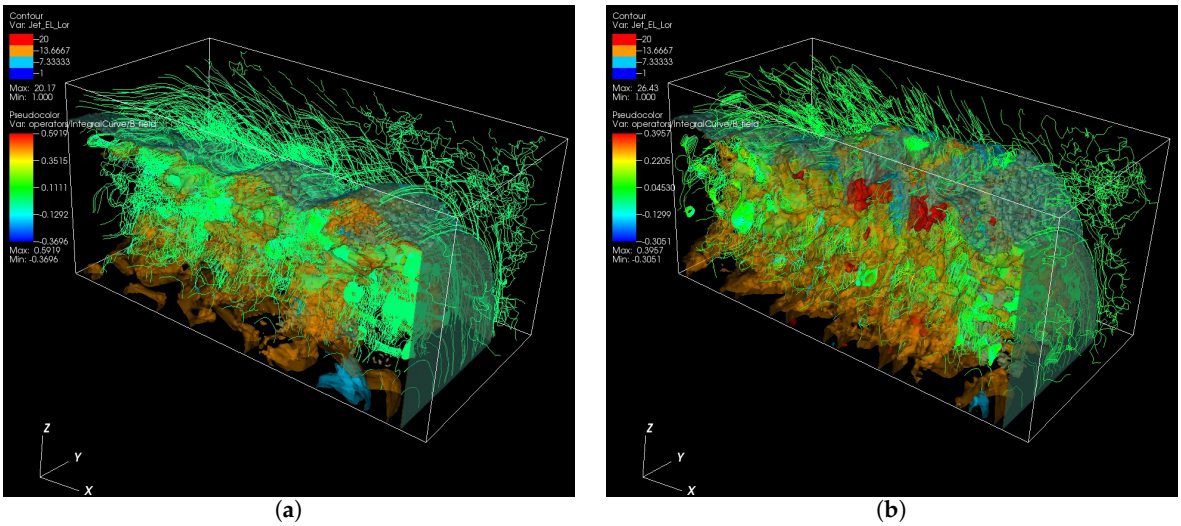


Figure 4. Panels show 3D iso-surface plots of the Lorentz factor of jet electrons for e^{-}–p^{+} (**a**) and $e^{\pm}$ (**b**) jets with $r_{\rm jet} = 120\Delta$ at time $t = 500\omega_{\rm pe}^{-1}$. The lines show the magnetic field stream lines in the quadrant of the front part of jets. The color scales for the contour (upper left) for (**a**,**b**) are red: 20.0; orange: 13.67; right blue: 7.33; blue: 1. The color scales of streaming lines are (**a**) (5.92, 3.52, 0.174, -1.29, -3.70) $\times 10^{-1}$, and (**b**) (3.96, 2.21, 0.453, -1.30, -3.05) $\times 10^{-1}$.

3. Discussion

The global jet simulations with large jet radii have shown the importance of a larger jet radius in RPIC simulations for in-tandem investigation of the macroscopic processes incorporated in RMHD simulations. As a result of mixed modes of generated instabilities, jet electrons in phase space show little or no bunching in comparison to those with a jet radius of $r_{\rm jet} = 20\Delta$, as shown in Figure 5a,b in a previous report [5]. Consequently, recollimation shocks occur rather in the center of jets, and this is dependent on the value of a in Equations (1) and (2). Further simulations with different values of a are required for investigating the evolution of kinetic instabilities in global jets.

These simulations show that the energy stored in helical magnetic fields is released as a result of the excitations of kinetic instabilities such as the kKHI, MI, and the Weibel instability with kink-like instability. Consequently, electrons are accelerated and turbulent magnetic fields are generated, which provide polarity.

MacDonald & Marscher [3] developed a radiative transfer scheme that allows the Turbulent Extreme Multi-Zone (TEMZ) code to produce simulated images of the time-dependent linearly and circularly polarized intensity at different radio frequencies. Using this technique with our simulation results, we have produced synthetic polarized emission maps that highlight the linear and circular polarization expected within the model. We will discuss these findings in a separate paper.

We plan to perform additional simulations using a larger jet radius and longer systems in order to investigate the full dynamics of jet evolution and interaction with ambient mediums through developing instabilities.

Supplementary Materials: The following are available online at www.mdpi.com/2075-4434/5/4/58/s1. Figure S1: Panels show iso-surface plots of the x component of current J_x in the $y-z$ plane for e^{-} –p^{+} (a) and $e^{\pm}$ (b) jet with $r_{\rm jet} = 120\Delta$ at $x = 380\Delta$ at time $t = 500\omega_{\rm pe}^{-1}$. For the $e^{\pm}$ (b) jet the patters of rings are generated outside of the jet by the kKHI. The arrows show the magnetic field strength in the $y-z$ plane.

Acknowledgments: This work was supported by NSF AST-0908010, AST-0908040, NASA-NNX09AD16G, NNX12AH06G, NNX13AP-21G, and NNX13AP14G grants. The work of J.N. and O.K. has been supported by Narodowe Centrum Nauki through research project DEC-2013/10/E/ST9/00662. Y.M. is supported by the ERC Synergy Grant "BlackHoleCam—Imaging the Event Horizon of Black Holes" (Grant No. 610058). M.P. acknowledges support through grant PO 1508/1-2 of the Deutsche Forschungsgemeinschaft. Simulations

were performed using the Pleiades and Endeavor facilities at NASA Advanced Supercomputing (NAS), using Gordon and Comet at The San Diego Supercomputer Center (SDSC), and using Stampede at the Texas Advanced Computing Center, which are supported by the NSF. This research was started during the program "Chirps, Mergers and Explosions: The Final Moments of Coalescing Compact Binaries" at the Kavli Institute for Theoretical Physics, which is supported by the National Science Foundation under Grant No. PHY05-51164. The first velocity shear results using an electron–positron plasma were obtained during the Summer Aspen workshop "Astrophysical Mechanisms of Particle Acceleration and Escape from the Accelerators" held at the Aspen Center for Physics (September 1–15, 2013).

Author Contributions: Ken-Ichi Nishikawa performed simulations, analyzed the data and prepared the manuscript; Yosuke Mizuno compared RMHD simulations; Jose L. Gómez contributed to comparing simulation results with observations; Jacek Niemiec contributed to modifying the code for this research; Oleh Kobzar modified the code for this simulation; Martin Pohl oversaw the simulation results; Jose L. Gómez contributed to comparisons with observations; Ioana Duţan performed some of the simulations for this research; Asaf Pe'er gave critical contributions for the physical interpretation; Jacob Trier Frederiksen contributed to critical discussions on this research; Åke Nordlund gave fruitful suggestions for this research; Charley White contributed to some of the simulations and discussions; Athina Meli gave a critical reading and discussion of this research; Helene Sol gave essential suggestions for this research; Philip E. Hardee gave theoretical contributions for this research; Dieter H. Hartmann gave useful discussions for this research.

Conflicts of Interest: The authors declare no conflict of interest.

References

1. Hawley, J.F.; Fendt, C.; Hardcastle, M.; Nokhrina, E.; Tchekhovskoy, A. Disks and Jets Gravity, Rotation and Magnetic Fields. *Space Sci. Rev.* **2015**, *191*, 441–469.
2. Pe'er, A. Energetic and Broad Band Spectral Distribution of Emission from Astronomical Jets. *Space Sci. Rev.* **2014**, *183*, 371–403.
3. Nicholas, R.; MacDonald, M.R.; Marscher, A.P. Faraday Conversion in Turbulent Blazar Jets. *arXiv* **2016**, arXiv:1611.09954.
4. Nishikawa, K.-I.; Frederiksen, J.T.; Nordlund, Å.; Mizuno, Y.; Hardee, P.E.; Niemiec, J.; Gómez, J.L.; Pe'er, A.; Duţan, I.; Meli, A.; et al. Evolution of Global Relativistic Jets: Collimations and Expansion with kKHI and the Weibel Instability. *Astrophys. J.* **2016**, *820*, 94–107.
5. Nishikawa, K.-I.; Mizuno, Y.; Niemiec, J.; Kobzar, O.; Pohl, M.; Gómez, J.L.; Duţan, I.; Pe'er, A.; Frederiksen, J.T.; Nordlund, Å.; et al. Microscopic Processes in Global Relativistic Jets Containing Helical Magnetic Fields. *Galaxies* **2016**, *4*, 38.
6. Duţan, I.; Nishikawa, K.-I.; Mizuno, Y.; Niemiec, J.; Kobzar, O.; Pohl, M.; Gómez, J.L.; Pe'er, A.; Frederiksen, J.T.; Nordlund, A.; et al. Particle-in-cell Simulations of Global Relativistic Jets with Helical Magnetic Fields. *New Front. Black Hole Astrophys. Proc. IAU Symp.* **2017**, *12*, 199–202.
7. Mizuno, Y.; Hardee, P.E.; Nishikawa, K.-I. Spatial Growth of the Current-Driven Instability in Relativistic Jets. *Astrophys. J.* **2014**, *784* 167–182.
8. Singh, C.B.; Mizuno, Y.; de Gouveia Dal Pino, E.M. Spatial Growth of Current-driven Instability in Relativistic Rotating Jets and the Search for Magnetic Reconnection. *Astrophys. J.* **2016**, *824*, 48.
9. Barniol Duran, R.; Tchekhovskoy, A.; Giannios, D. Simulations of AGN jets: Magnetic kink instability versus conical shocks. *Mon. Not. R. Astron. Soc.* **2017**, *469*, 4957–4978.
10. Mizuno, Y.; Gómez, J.L.; Nishikawa, K.-I.; Meli, A.; Hardee, P.E.; Rezzolla, L. Recollimation Shocks in Magnetized Relativistic Jets. *Astrophys. J.* **2015**, *809*, 38.

Sample Availability: Data (vtk) for VisIt and ParaView are available upon the request.



© 2017 by the authors. Licensee MDPI, Basel, Switzerland. This article is an open access article distributed under the terms and conditions of the Creative Commons Attribution (CC BY) license (http://creativecommons.org/licenses/by/4.0/).